J. Comp. App. Res. Mech. Eng. Vol. 15. No. 1, pp. 75-86, 2025 *DOI: 10.22061/jcarme.2025.11625.2555*

Journal of Computational and Applied Research in Mechanical Engineering

jcarme.sru.ac.ir

SRTTU

JCARME

ISSN: 2228-7922

Research paper

Surface acoustic waves and Chevron pattern, a solution for density-based cell separation

A. A. Naseri and N. Naserifar*

Department of Mechanical Engineering, K. N. Toosi University of Technology, Tehran, Iran.

Article info:

Article history:

Received: 23/01/2025

Revised: 07/11/2025

Accepted: 09/11/2025

Online: 11/11/2025

Keywords:

Cell separation,

Acoustics,

Buoyancy,

Density-based,

Chevron pattern.

***Corresponding author:**
naserifar@kntu.ac.ir

Abstract

Cancer is a common and often devastating disease affecting many individuals. This condition is frequently perceived as incurable; however, scientific advancements have shown that most cancers are treatable if detected early. The first step in diagnosing cancer is often identifying circulating tumor cells in the bloodstream. Separator devices are employed for the identification of cancer cells. Currently utilized devices are often bulky and marker-based and may come with a biohazard exposure risk. The advancement of micro-electro-mechanical systems (MEMS) has given rise to smaller devices capable of markerless separation; however, these devices have not yet attained the performance level of conventional devices. Designing a device that can reliably isolate cancer cells with a high degree of confidence is crucial. In this study, a method is presented for model preparation capable of simulating multiple physics. Subsequently, an optimization process is introduced for mesh size. It is aimed to investigate the design parameters for a novel cell separation device based on buoyancy and a Chevron channel. This device has the potential to increase the purity of separators by 10% in overall acoustic pressure and decrease shear drag. If properly aligned, the Chevron channel flow pattern can contribute to cell separation of acoustic radiation force or counteract it if necessary. Utilizing buoyancy force for cell separation based on cell density is a prominent feature of acoustic-Chevron separator devices. Finally, Chevron channel capabilities and design constraints are discussed.

1. Introduction

Efficient isolation of rare circulating tumor cells (CTCs) from blood remains a significant challenge in current cell separation technologies. Existing methods often rely on complex labeling protocols, suffer from low throughput, or compromise cell viability, limiting their utility in clinical and research settings. There is a clear need for label-free, high-throughput, and biocompatible separation methods that can preserve the physical and biological integrity of target cells while ensuring sufficient purity and recovery. CTCs, which shed from primary tumors into the bloodstream, provide valuable insight into cancer progression and metastasis [1]. Their isolation enables molecular characterization, which is vital for early diagnosis, personalized treatment, and monitoring of therapeutic outcomes [2].

Traditional techniques, including those using biomarkers, require additional steps to remove the labels before downstream analysis, potentially damaging cells or affecting viability [3].

Microfluidic-based passive separation methods, grouped into microfilter design, hydrodynamic forces, and deterministic lateral displacement (DLD), involve channel design and fluid property manipulation. Microfilters can separate cells by size despite complexity and issues like low throughput and clogging.

Hydrodynamic forces, induced by channel shapes like Dean Flow and Pinch Flow channel design, offer high throughput and simplicity, but struggle to isolate a single cell type. Finally, DLD's effectiveness varies across studies [4].

Acoustophoresis is a technique harnessing the power of acoustic forces to manipulate droplets on surfaces or cells within fluid-filled channels. By applying sound waves, this method enables precise control over the displacement of droplets or cells, ensuring minimal impact on cell vitality. Acoustophoresis eliminates the need for external markers, offering a label-free and bio-compatible approach to separation. Its ability to discriminate based on density and cell properties further enhances its versatility, making it a promising tool in biomedical applications [3, 5].

Biomarkers may simplify cell separation, but for further analysis of CTC, these markers must be first removed from the cell. This process, which can be complex or even impossible, also impacts cell viability [1].

Numerous efforts have been made in recent years to enhance the performance of acoustic cell separators. Some researchers focus on improving wave propagation, which could involve using different piezoelectrics or modifying the crystal cut. In 2020, Zhang *et al.* [6] found that on Lithium Niobate ($LiNbO_3$) substrate, while the x-axis at a 128-degree cut is the best angle for acoustic wave propagation, a 154-degree cut is one where wave propagation in any direction can yield the same result .

Other researchers have also attempted to improve the Interdigital Transducer (IDT) design for optimum acoustic pressure [7].

Other researches involve the arrangement and design of transducers to control wave propagation direction, consequently controlling the direction of cell displacement [8].

In acoustic separation, to help with dilution issues, the process is divided into two stages: center concentration (or aligning stage) and separation [3, 9].

In the aligning stage, acoustic force pushes cells toward the center of the channel. In the separation stage, this force keeps target cells at the center while relocating other cells to the sides of the channel and vice versa. In another study on cell sorting, Liu *et al.* used only one pair of IDTs but implemented two different channel designs, referred to as sequential and direct. They successfully sorted three different types of particles by adjusting the peak-to-peak voltage of the IDT. The sorting process achieved a reported purity ranging from 83.49% to 94.3% [10].

Numerous studies in the field of micromixers have examined Chevron-patterned channels [11]. However, in the field of cell separators, Researchers overlooked the ability of particle separation using these channels. To the best of our knowledge, in 2008, Hsu *et al.* [12] were the first to demonstrate the separation ability of a herringbone-patterned channel. They demonstrated particle separation based on density difference and buoyancy force. Buoyancy-based separation techniques, such as BACS, offer a novel approach to cell separation. Buoyancy Activated Cell Sorter (BACS) employs biomarkers, centrifugation, and rest time for separation.

Other buoyancy-driven methods rely on bubbles or shear stress for differentiation. Yet, both bubbles and shear stress can compromise cell viability [13].

In 2013, Sheng *et al.* [14] successfully isolated CTCs with the help of adhesive material on the ceiling of a Chevron-patterned channel. They optimized purity and throughput through channel design. Later, in 2016, Wang *et al.* [15] demonstrated increased adhesion with a non-symmetrical Chevron design.

In 2017, Ung *et al.* [16] used a slanted groove to significantly boost the throughput of a cell separation device powered by a single IDT, rendering it comparable to widely used devices like FACS.

2. Methods

2.1. Separation mechanism

A typical SAW-based cell separation device has three components: a substrate, a pair of IDTs, and a microchannel. Fig. 1(a) illustrates this device. In this acoustic cell sorter, all the cells are concentrated in the channel center using sheath flows before the separation level. To counter the dilution issue of the sample, sheath flows can be replaced by another pair of IDTs. A Chevron channel can be utilized in different stages of such a device. Fig. 1(b) shows different proposed design choices with a Chevron channel.

The Chevron channel can be properly aligned and used for separation and concentration stages. Also, it can be added as a purification stage at the end of the channel. Fig. 1(c) is a schematic of a microchannel with Chevron grooves on its ceiling. This pattern directs fluid flow toward the apex of the pattern. The Chevron pattern generates an interesting flow inside the channel. Fig. 1(d) shows the result of simulating a fluid flowing inside this channel and illustrates the acting forces on a particle. The resulting forces on particles generate two trap zones; Chevron's apex region traps Low-density particles, and the pattern's wings trap high-density particles [12].

IDTs are two comb-like structures of evenly spaced metallic electrodes (fingers) on a piezoelectric substrate. The piezoelectric substrate periodically expands and contracts when electrodes are under alternating voltage. This periodic expansion and contraction generate a SAW within the solid medium. The SAW then propagates along the surface of the substrate. Eq. (1) is the resulting electrical potential of such a device [5].

$$\phi^{+}(z)=\mu_s V_0 \sum_{n=0}^{N_f-1}(-1)^n e^{-jnkd/2} \tag{1}$$

ϕ^{+} represents electrical potential, μ_s denotes substrate constant, V_0 is continuous wave voltage, N_f indicates the number of fingers, and d denotes the distance between two consequent fingers.

Piezoelectric is a type of material that, in an electrical field, generates stress/strain. Eq. (2) defines the stress-charge form of the piezoelectric constitutive equation.

$$\begin{aligned} T_I &= c^{E}{}_{IJ} S_J - e_{Ij} E_j \\ D_i &= \varepsilon_{ij}{}^{S} E_j + e_{iJ} S_J \end{aligned} \tag{2}$$

where T is the stress tensor, c is the stiffness matrix, E is the electric field, S is the strain matrix, e is the coupling properties, D is the electric displacement field, and ε is the permittivity. I, J, i, and j are reduced matrix indices.

Then, the generated SAW travels through the substrate at the speed of sound until it meets the fluid medium of the microchannel. Eq. (3) expresses acoustic wave propagation in a fluid medium [17].

$$\nabla.\left(-\frac{1}{\rho_c}\left(\nabla p_t - q_d\right)\right) - \frac{k_{eq}{}^2 p_t}{\rho_c} = Q_m \tag{3}$$

p_t denotes the total pressure, ρ_c represents the fluid density at the speed of sound, k_{eq} is the wave number, and Q_m indicates the monopole domain source.

At the solid–fluid interface, a sound-hard boundary condition is applied. Under this condition, the normal derivative of the acoustic pressure is set to zero, corresponding to zero normal particle velocity [17].

The floating particles in the fluid medium are affected by all sorts of forces: drag, lift, Saffman lift, buoyancy, gravity, and acoustic force. By assuming a spherical shape for particles, the lift force can be negligible. Also, the Saffman lift is a force that prevents particles from approaching channel boundaries.

Analyzing the effects of microfluidic phenomena like the Saffman lift is beyond the scope of this research, so by assuming a minimum distance from channel boundaries, the Saffman lift can be negligible, too. The drag and buoyancy forces in a fluid medium are extensively discussed and examined in fluid mechanics textbooks [18].

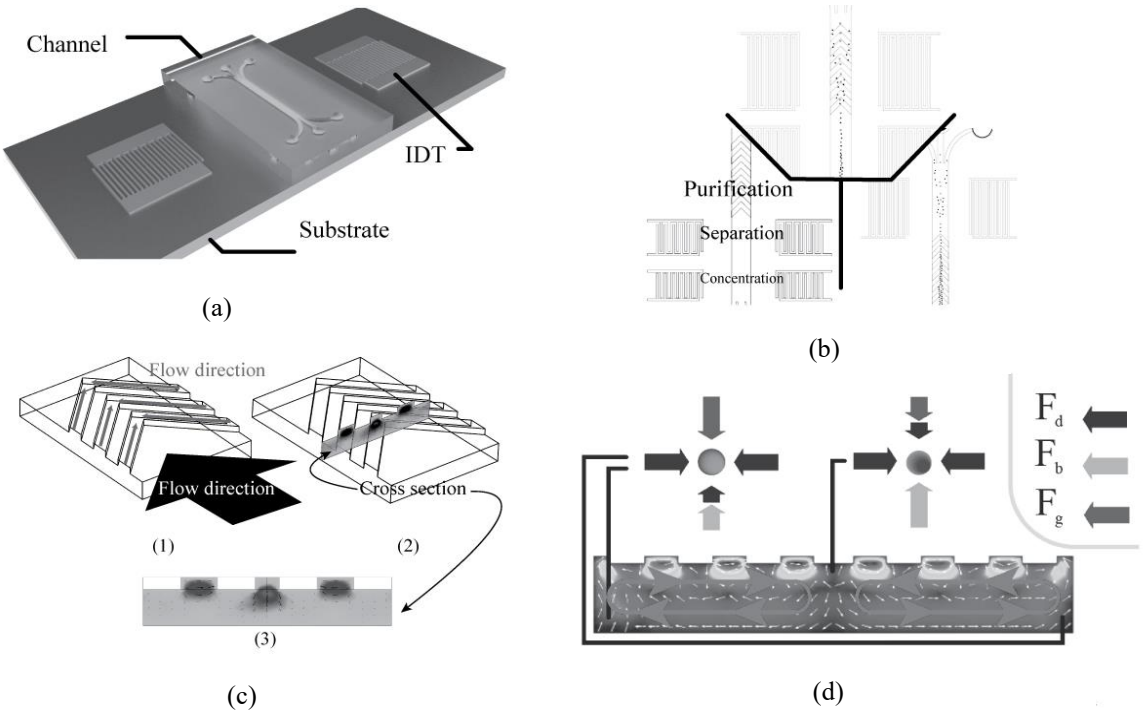

Fig. 1. (a) Typical SAW-based cell separator. Individual components are IDT, substrate, and microchannel; (b) proper alignment of the chevron channel: The top section involves coupling the chevron with SAW in the separation stage. On the left, the chevron is utilized as an extra purification stage, and on the right, it serves as a concentration stage; (c) flow direction and shear flow formation in a chevron channel; (d) the acting forces on a cell floating in two trapping zones formed by the chevron pattern. One zone forms on the apex and another one on the wings of the chevron pattern.

In this study, the governing equation of these forces is as follows:

A drag force F_d on a floating particle of radius R in a fluid with viscosity η can be defined as Eq. (4).

$$F_d = -6\pi R\eta\left(v_m - v_p\right) \tag{4}$$

v_m and v_p are velocities of medium and particle, respectively.

Buoyancy is an upward force exerted on an object immersed in a fluid by the density difference between the object and the fluid. Eq. (5) indicates the resulting buoyancy force F_b on the particle of radius R in a medium with ρ_m density.

$$F_b = \frac{4}{3}\pi R^3 \rho_m g \tag{5}$$

where g represents the gravitational constant. In this study, gravity force (Fg) affecting particle density ρ_p is considered as Eq. (6).

$$F_g = \frac{4}{3}\pi R^3 \rho_p g \tag{6}$$

Eq. (7) describes the acoustic radiation force (F_r) acting on a particle [9, 19].

$$F_r = -\left(\frac{\pi p_0^{\,2} V_p \beta_m}{2\lambda}\right)\phi(\beta,\rho)\sin(2kx) \tag{7}$$

p_0, V_p, λ, k, and x represent fluid's acoustic pressure, particle volume, wavelength, wave number, and distance between particle and pressure node, respectively. Note that ϕ in this equation indicates acoustic contrast factor and is a function of density (ρ) and compressibility (β). Eq. (8) expresses the acoustic contrast factor.

$$\phi = \frac{5\rho_p - 2\rho_m}{2\rho_p + \rho_m} - \frac{\beta_p}{\beta_m} \quad (8)$$

In Eq. (8) ρ_p and β_p are particle density and compressibility, and ρ_m and β_m are medium density and compressibility, respectively. If this factor for a particle is positive, then the particle is attracted toward pressure nodes, and if it is negative, the particle tends to move toward the pressure antinode.

Here, a pipeline is proposed to find the best mesh quality and polygon count regarding the computational resources. In this pipeline, first, parts of the mesh are identified that require finer polygons. Second, a ratio to each part is assigned based on available computational resources. Third, while monitoring the skewness results of Eq. (9) [20], polygon counts for important parts are increased.

$$e_{skewness} = 1 - \max\left(\frac{\theta - \theta_e}{180 - \theta_e}, \frac{\theta_e - \theta}{\theta_e}\right) \quad (9)$$

which θ denotes the angle between two edges of the element, and θ_e indicates the ideal angle between those edges.

This process repeats until the desired criteria are satisfied and the maximum number of elements does not exceed the maximum computational resources. The chosen criteria are as follows: 99% of polygons above 0.5 skewness, 70% above 0.7 skewness, and no polygon is allowed below 0.2 skewness. Fourth, the result of Eq. (10) must converge [20, 21]. These four steps result in an optimized mesh size.

$$f_{conv} = \sqrt{\frac{\int \left(g - g_{ref}\right)^2 dxdydz}{\int g_{ref}\, dxdydz}} \quad (10)$$

where g replaces one parameter of simulation parameters, and g_{reg} becomes the result of that parameter using the smallest possible mesh.

2.2. Methodology

As observed in the preceding section, various physical phenomena are involved in the Chevron channel separator formation. Due to the nature of the Chevron pattern shape, a 3-dimensional simulation is inevitable, too.

Independent modeling and validation of each physics ensures precise validation. Validation takes place in a step-by-step fashion in which a 2d model, specifically designed for simulating a SAW separator by a pair of IDTs. This model is a direct replica of the proposed model by Shamloo and Boodaghi [19]. Then, another model addresses the same simulation in a 3d environment.

The outcomes of these two simulations are compared to the results of Shamloo and Boodaghi [19] to validate the simulation used in this study. In these models, feature sizes and wavelength determine the region's importance in meshes. These two models are depicted in Fig. 2. Finally, a fluid simulation based on Hsu and colleagues' study is used to validate the fluid flow simulation [12]. A part of this simulation is shown in Fig. 1(d).

Fig. 2(c) illustrates the proposed model. This model is used for SAW simulation to investigate the effects of SAW generated in a Chevron channel. Initially, a repeatable domain was intended to be created, but because of the reasons explained in the discussion section, it was not possible. Finally, a model for fluid flow simulation is considered to analyze Chevron channel's design parameters. These parameters are pretty simple, but they shape the flow pattern in the channel. Fig. 2(d) depicts the Chevron channel's height a and width w. Also, in this study, a cubic Chevron means that the width of the channel is equal to its height ($w = a$).

It is important to note that the simulation results of one physics domain serve as inputs to subsequent simulations. First, the electrical simulation yields piezoelectric displacement, which is then used to compute the acoustic pressure in the solid domain. This solid-state acoustic pressure is subsequently applied to determine the resulting acoustic field in the fluid domain. Finally, the fluid dynamics simulation incorporates both the fluid forces and the acoustic field to evaluate the total force distribution. Simulations were performed using COMSOL Multiphysics version 5.4.

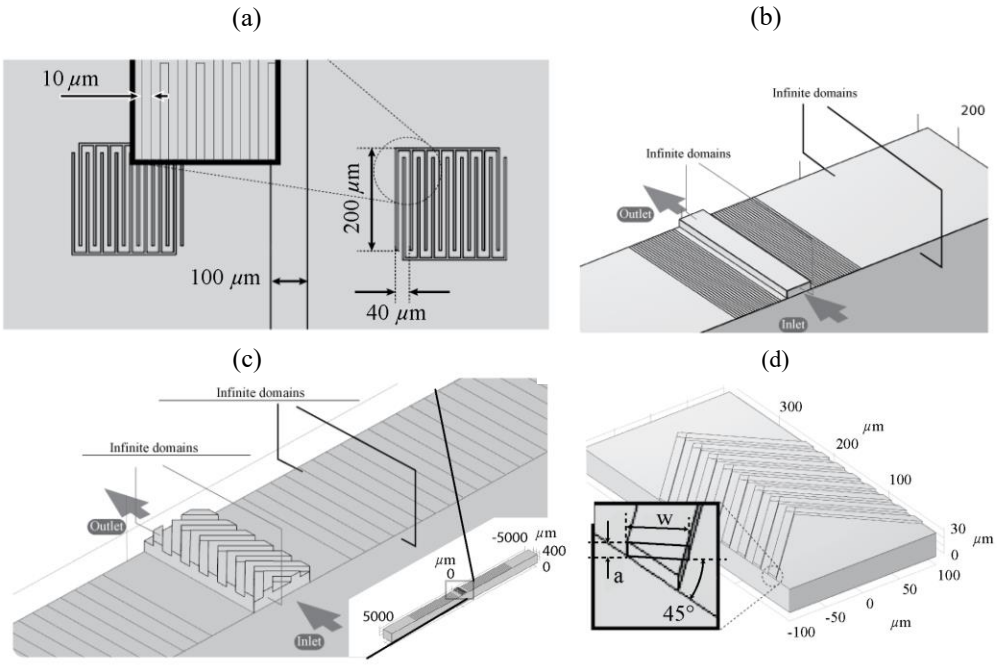

Fig. 2. (a) 2d model of a typical cell separator. The model's dimensions are derived from the works of Shamloo and Boodaghi to simulate SAW generated by IDTs [19]; (b) The model used for 3d simulation of a SAW separator: (c) Chevron model setup was used for this study. The constraints shown as infinite domains were initially considered repeatable domains. This assumption is incorrect due to acoustic field results shown in the Discussion Section; and (d) A model used for fluid flow simulation. The displayed dimensions for the channel remain untouched, while the dimensions for the chevron are modifiable. Width w and height a of the chevron are calculated from a 45-degree cut.

3. Results and discussion

3.1. Acoustic radiation force

The mesh size was selected first. The previous section covered the process of mesh size selection. However, considering wavelength and frequency effects, higher-order elements are used. But these demand more computing power. To balance, higher-order elements are assigned for mechanical, electrical, and acoustic physics, and lower-order elements for fluid flow and particle tracing to save computational resources. Table 1 shows the mesh divisions used in the 3d Chevron model. The first index of this table is based on the computing power limits, and the convergence function shown in Eq. (9) is calculated for four different parameters.

The parameters used for the convergence function are acoustic pressure, mechanical stress, electrical potential, and fluid flow velocity.

Fig. 3 shows the resulting convergence of Table 1. . Also, the same procedure is undergone by other models used in this study.

Analyzing wave properties in the piezoelectric shows the correct mode shape. These properties include wavelength, attenuation, and strain energy [5]. In a SAW, the strain energy diminishes after one wavelength deep inside a solid body.

Material properties used in this study are as follows. YX-128-degree $LiNbO_3$ piezoelectric with a reported 3992 m/s sound wave speed [22]. The stiffness matrix used in this study can be found in Ref [23].

The Fluid medium is water with a density of 0.99987 grams per cubic centimeter, and in the particle tracing simulation, particles are polystyrene with a density of 1.05 grams per cubic centimeter [18]. The material properties and stiffness matrix are listed in Tables 2 and 3, respectively.

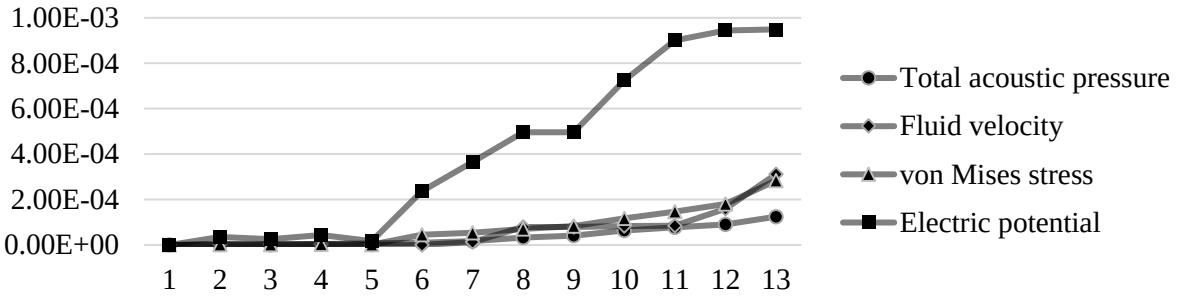

Fig. 3. Convergence for individual physics. X axis is the index for mesh size table. Y axis is dimensionless see the convergence equation (Eq. (10)).

Table 1. Mesh size table for the 3D acoustic model (Chevron). The optimal variation was selected based on skewness, computational resources, and convergence criteria, as explained in Section 2.1.

IDT max/min element size (μm)	Channel length/height/width number of elements	Channel division ratio	Channel max/min element size (μm)
5/2	140/20/60	12	5/2
5/2	130/18/50	12	5/2
5/2	120/15/40	12	5/2
5/2	100/10/20	12	5/2
5/2	70/8/10	12	10/5
10/5	70/8/10	12	10/5
10/5	50/4/5	12	10/5
10/5	40/4/2	10	15/10
15/10	40/4/2	10	15/10
15/10	10/3/2	10	15/10
15/10	10/3/2	10	15/10
15/10	10/2/2	8	30/15
15/10	10/1/1	8	30/15

Table 2. Material properties.

Sound wave speed in YX-128-degree LiNbO3 (m/s)	Density of water (g/cm^3)	Density of polystyrene (g/cm^3)	Dynamic viscosity of water ($Pa.s$)
3992 [22]	0.99987 [18]	1.05 [18]	10^{-3} [12]

Table 3. Elastic stiffness coefficients ($\times 10^{11} N/m^2$) at constant electric field [23].

Parameter	c_{11}	c_{12}	c_{13}	c_{14}	c_{33}	c_{44}
c^E	2.030	0.573	0.752	0.085	2.424	0.595
c^E	2.03	0.53	0.75	0.09	2.45	0.60
c^E	2.0	0.54	0.6	0.08	2.43	0.60
c^E	2.06	–	–	–	2.36	–

fter simulating the 2d and 3d SAW model by applying an alternating voltage of 5 volts to IDT domains, the acoustic pressure results at 7.33 MHz shape mode and acoustic pressure distribution demonstrate a good correlation with the findings by Shamloo and Boodaghi [19] (see Supplementary 1 for a detailed comparison).

3.2. Hydrodynamic forces

A replication of Hsu *et al.*'s work [12], which was simulated for this study, shows the trapping zones mentioned in the previous section, and the present simulation's flow velocity matches that of Hsu *et al.*'s report.

3.3. Chevron's design parameters

The separation mechanism of a Chevron channel is explained in the section Separation Mechanism. Also, the drag force has a direct correlation with fluid velocity. So, it is reasonable to speculate that increasing fluid velocity will boost the separation power. To analyze the effect of each parameter, the changes in one parameter is assessed while keeping another constant. First, the height of the Chevron is increased by one micron while the width is kept at 10 microns. Second, at a constant height of 5 microns, the channel width is increased by 1 micron. Third, both the height and the width are equal and equally increased. The results of fluid flow simulation for the three mentioned steps and maximum fluid velocity for all simulations are consolidated and presented in Fig. 4.

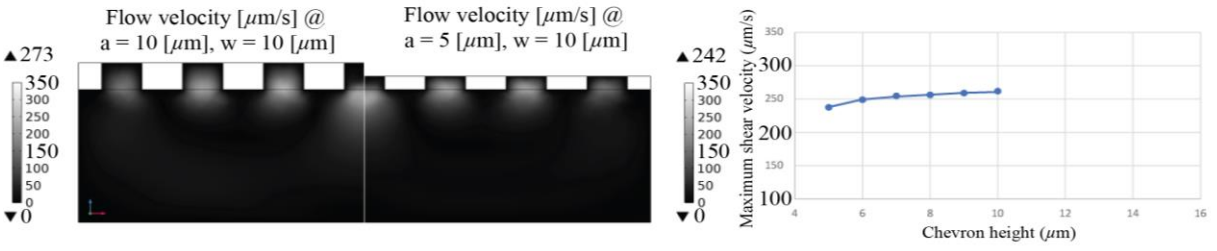

(a)

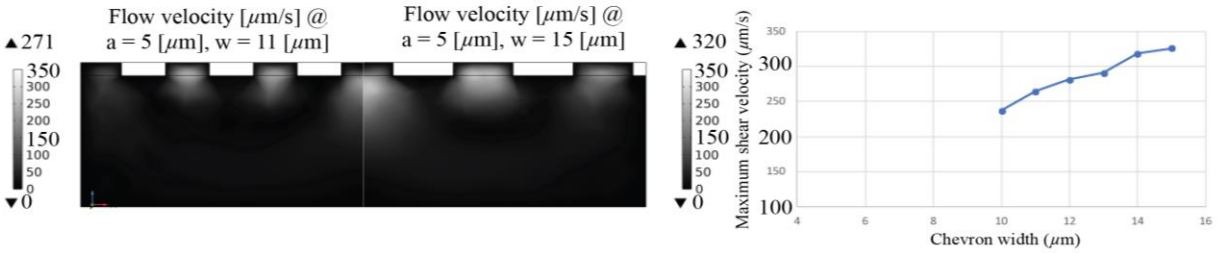

(b)

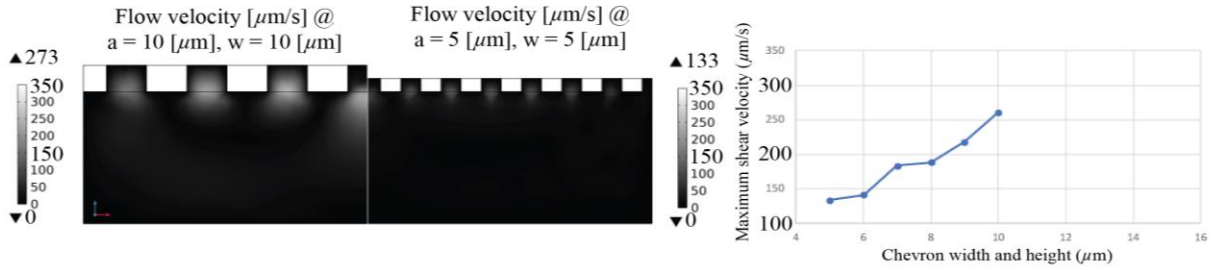

(c)

Fig. 4. Results of fluid simulations: (a) increasing Channel height at a constant width of 10μm; (b) increasing channel width at a constant height of 5μm; and (c) increasing cubic ($w = a$) chevron.

3.4. Fluid velocity in Chevron channel

From Fig. 4, it can be inferred that increasing the height of the Chevron has little impact on increasing the fluid velocity, or it is better to say it has a negligible effect. Meanwhile, with a change in the width of the channel, a significant increase in the fluid flow velocity is observed.
Therefore, increasing the width of the slot can be chosen as a parameter with a more pronounced effect. Results for cubic Chevron simulations also back this idea up.

3.5. Acoustic pressure and acoustic radiation force in a Chevron channel

With validated simulation steps in the previous section, three devices with different channel designs are modeled here, making further SAW effects investigations possible. These designed channels are one simple typical channel and two Chevron channels, one with Chevron grooves carved from the typical channel and the other with added Chevron volume on top of the typical channel Input alternating voltage on IDTs is 5 volts again, and the same pipeline is used for mesh size optimization.
As is illustrated in Fig. 5, the Chevron channel has an interesting placement of the pressure node and antinode. Although it follows the same symmetrical pattern and is experiencing a difference in overall acoustic pressure level, the pressure spectrum difference toward the apex direction is much higher.
By categorizing Chevron channels into high-volume and low-volume groups and then comparing them with typical channels, the acoustic pressure level drops as volume decreases.
Examining cubic and Chevron channels together indicates a damping effect toward the tail of the pattern, while a smaller channel profile mitigates this effect. The middle section view of the Chevron channels indicated in Fig. 5 shows that the acoustic pressure distribution remains almost intact along the height (z-axis) of the channel.

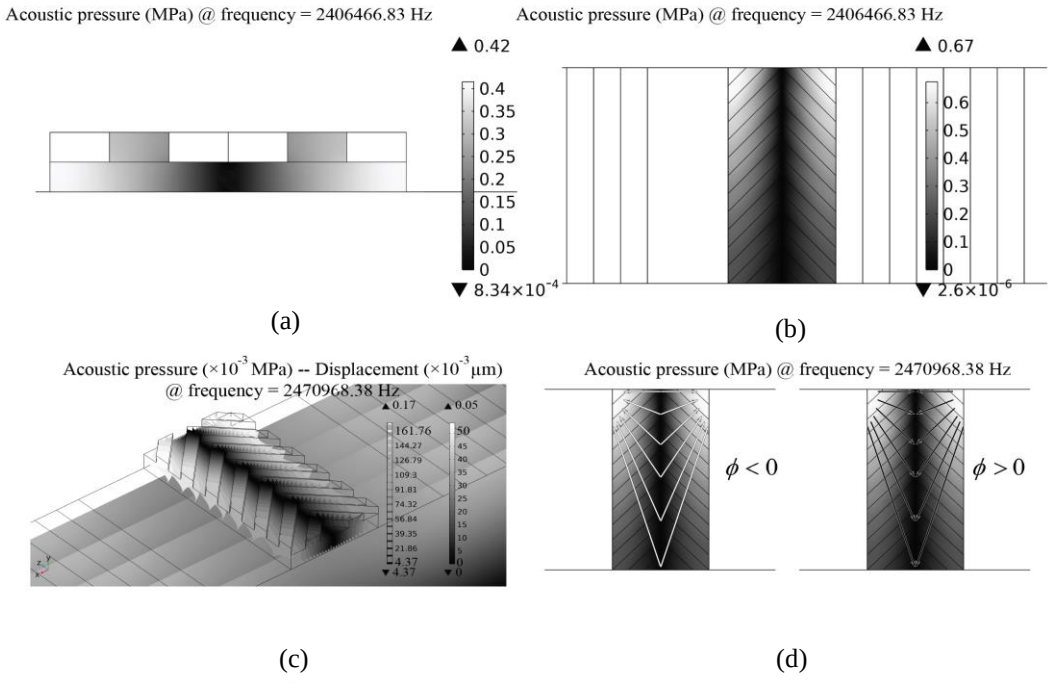

Fig. 5. Acoustic pressure results in the chevron model: (a) A cross-section of the channel; (b) surface plot top view of the chevron channel; (c) shows the corresponding mode shapes used to find the right eigenfrequency in which the Rayleigh surface wave propagates; and (d) acoustic radiation force field schematic.

In a typical rectangular channel, the acoustic pressure field is independent of channel height [9], while in a Chevron channel with carved Chevrons from the channel ceiling, the maximum acoustic pressure increases. Due to this nonuniform pressure distribution along the channel length, a repeated domain was not applicable for the Chevron model. In our results, acoustic pressure in the Chevron channel is associated with a 10% increase compared to the typical rectangular channel.

The acoustic contrast factor (Eq. (8)) of a medium-particle pair affects the force direction in an acoustic field. Fig. 5(d) is a schematic of this direction based on the sign of this factor. This force can slow down or speed up certain particles or cells in the channel.

In the particle tracing results, particles floating in a Chevron channel move toward these trap zones. Also, there is a slight displacement toward the center when the IDTs are on. In other words, this displacement confirms the acoustic radiation force acting on polystyrene particles.

Another intriguing result of the Chevron channel's particle tracing is that the particle forward velocity at the center of the channel is slightly lower. Finally, a long channel is needed for an effective separation, only by a Chevron channel.

3.6. Device design

As a brief review, a SAW separator apparatus consists of two stages called queueing and separation. Fig. 1(b) shows schematics of different separators with a Chevron channel. For the concentration stage, IDTs are still a viable choice. For our first design, in the separation stage, instead of IDT, a Chevron channel is replaced with a density-based separation. This design appears to have the potential to separate two particle types despite medium density importance with a flow velocity as low as 20 microns per second, as reported by Hsu *et al.* [12]. This low flow velocity is due to the uniform flow requirement and consequent low Reynolds number [18].

In another design, the separation stage of a typical acoustic-based separator is coupled with a Chevron channel. Like the first design, fluid density plays a crucial role in the separating mechanism of the Chevron channel. One of the forces that a typical SAW must counteract is the fluid drag force [24]. This design emerges to help the drag issue. The shear flow of a Chevron channel can be used as a facilitator to overcome drag forces, and drag reduction can lead to a higher overall purity of outlets. To reduce drag, raising shear velocity can be a good idea. Then, heightening the Chevron's ceiling increases the shear velocity profile, but at the cost of lower acoustic pressure. The left design of Fig. 1(b) adds a purification stage to the typical two-stage acoustic separator. The longer the Chevron channel, the more purified the storage will be. If the fluid medium density is unmodifiable, or the density difference between two particle types is thin, a device design with a Chevron channel used for its concentration stage can be used to reduce the fabrication process costs of IDT.

4. Conclusions

Chevron patterns are capable of density-based separation, and they can be effectively integrated within an acoustic field to improve separation performance. An effective separator design depends on several factors, including channel height and fluid properties. Particles are either pushed toward the surface or sunk to the depth primarily by the fluid's properties. These displacements require a fluid density difference between the target particles and their medium. Also, the trade-off between channel height and acoustic pressure is quite appealing and can be used to target a specific cell. The notable positioning of pressure nodes and antinodes and their applications can be an interesting future study. Future work should focus on experimental validation to further substantiate and extend the findings of this study.

References

[1] C. Yang, B. R. Xia, W. L. Jin, and G. Lou, “Circulating tumor cells in precision oncology: clinical applications in liquid biopsy and 3D organoid model,” *Cancer Cell Int.*, Vol. 19, No. 1, pp. 1–13, (2019),

[2] World Health Organization, "Cancer." Accessed: Nov. 29, 2021. [Online]. Available: https://www.who.int/news-room/fact-sheets/detail/cancer

[3] C. Wyatt Shields IV, C. D. Reyes, and G. P. López, "Microfluidic cell sorting: a review of the advances in the separation of cells from debulking to rare cell isolation," *Lab Chip*, Vol. 15, No. 5, pp. 1230–1249, (2015).

[4] S. A. Mateen and K. S. Bhole, "A review on microfluidic devices for separation of blood constituents," *IOP Conf. Ser.: Mater. Sci. Eng.*, Vol. 810, No. 1, p. 012024, (2020).

[5] D. S. Ballantine, R. M. White, S. J. Martin, A. J. Ricco, E. T. Zellers, G. C. Frye and H. Wohltjen, *Acoustic wave sensors : theory, design, and physico-chemical applications*. Academic Press, (1997).

[6] N. Zhang, J. Mei, T. Gopesh, and J. Friend, "Optimized, Omnidirectional Surface Acoustic Wave Source: 152° Y-Rotated Cut of Lithium Niobate for Acoustofluidics," *IEEE Trans. Ultrason. Ferroelectr. Freq. Control*, Vol. 67, No. 10, pp. 2176–2186, (2020).

[7] X. Chen, M. A. Mohammad, J. Conway, B. Liu, Y. Yang, and T.-L. Ren, "High performance lithium niobate surface acoustic wave transducers in the 4–12 GHz super high frequency range," *J. Vac. Sci. Technol. B*, Vol. 33, No. 6, pp. 401–412, (2015).

[8] P. Kang, Z. Tian, Sh. Yang, W. Yu, H. Zhu, H. Bachman, Sh. Zhao, P. Zhang, R. Zhong and T. J. Huang, "Acoustic tweezers based on circular, slanted-finger interdigital transducers for dynamic manipulation of micro-objects," *Lab Chip*, Vol. 20, No. 5, pp. 987–994, (2020).

[9] J. Shi, H. Huang, Z. Stratton, Y. Huang, and T. J. Huang, "Continuous particle separation in a microfluidic channelvia standing surface acoustic waves (SSAW)," *Lab Chip*, Vol. 9, No. 23, pp. 3354–3359, (2009).

[10] G. Liu, H. H. Li, H. Zhao, X. Li, H. Tang, Zh. Li, Zh. Yang and Y. zhang, "Effects of two surface acoustic wave sorting chips on particles multi-level sorting," *Biomed. Microdevices*, Vol. 21, No. 3, pp. 1–15, (2019).

[11] B. Hama, G. Mahajan, P. S. Fodor, M. Kaufman, and C. R. Kothapalli, "Evolution of mixing in a microfluidic reverse-staggered herringbone micromixer," *Microfluid. Nanofluid.*, Vol. 22, No. 5, pp. 1–14, (2018).

[12] C. H. Hsu, D. Di Carlo, C. Chen, D. Irimia, and M. Toner, "Microvortex for focusing, guiding and sorting of particles," *Lab Chip*, Vol. 8, No. 12, pp. 2128–2134, (2008).

[13] Y. R. Liou, Y. H. Wang, C. Y. Lee, and P. C. Li, "Buoyancy-Activated Cell Sorting Using Targeted Biotinylated Albumin Microbubbles," *PLoS One*, Vol. 10, No. 5, p. e0125036, (2015).

[14] W. Sheng, O. O. Ogunwobi, T. Chen, J. Zhang, T. J. George, Ch. Liu and H. Fan*t al.*, "Capture, release and culture of circulating tumor cells from pancreatic cancer patients using an enhanced mixing chip," *Lab Chip*, Vol. 14, No. 1, pp. 89–98, (2013).

[15] S. Wang, S. Sohrabi, J. Xu, J. Yang, and Y. Liu, "Geometry design of herringbone structures for cancer cell capture in a microfluidic device," *Microfluid. Nanofluid.*, Vol. 20, No. 11, pp. 1–11, (2016).

[16] W. L. Ung, K. Mutafopulos, P. Spink, R. W. Rambach, T. Franke, and D. A. Weitz, "Enhanced surface acoustic wave cell sorting by 3D microfluidic-chip design," *Lab Chip*, Vol. 17, No. 23, pp. 4059–4069, (2017).

[17] A. D. Pierce and P. W. Smith, *Acoustics: An Introduction to Its Physical Principles and Applications* , Vol. 34, No. 12. AIP Publishing, (1981).

[18] B. R. Munson, P. M. Gerhart, A. L. Gerhart, J. I. Hochstein, D. F. Young, and T. H. Okiishi, *Munson, Young, and Okiishi's Fundamentals of fluid*

mechanics. John Wiley & Sons: New Jersey, (2013).
[19] A. Shamloo and M. Boodaghi, "Design and simulation of a microfluidic device for acoustic cell separation," *Ultrasonics*, Vol. 84, pp. 234–243, (2018).
[20] J. D. , Jr. Anderson, *Computational Fluid Dynamics: The Basics with Applications*. McGraw-Hill, USA, (1995).
[21] W. H. Press, S. A. Teukolsky, W. T. Vetterling, and B. P. Flannery, *Numerical Recipes : The Art of Scientific Computing*, 3rd ed. Cambridge University Press, (2007).
[22] B. A. Auld, *Acoustic fields and waves in solids. Vol. I.*, 2nd ed. Krieger Publishing Company: Malabar, FL, (1990).
[23] R. S. Weis and T. K. Gaylord, "Lithium niobate: Summary of physical properties and crystal structure," *Appl Phys A*, Vol. 37, No. 4, pp. 191–203, (1985).
[24] M. Wu, A. Ozcelik, J. Rufo, Z. Wang, R. Fang, and T. Jun Huang, "Acoustofluidic separation of cells and particles," *Microsyst. Nanoeng.*, Vol. 5, No. 1, pp. 1–18, (2019).

How to cite this paper:

A. A. Naseri and N. Naserifar, "Surface acoustic waves and Chevron pattern, a solution for density-based cell separation*", J. Comput. Appl. Res. Mech. Eng.*, Vol. 15, No. 1, pp. 75-86, (2025).

DOI: 10.22061/jcarme.2025.11625.2555

URL: https://jcarme.sru.ac.ir/?_action=showPDF&article=2444